



## Research Paper

# Experimental and numerical study on the soil arching effect caused by deep-buried shield tunneling

Xu Song<sup>a</sup>, Chang-Wei Miao<sup>a</sup>, Ren-Peng Chen<sup>b,c,\*</sup>, Xiao-Ning Deng<sup>a</sup>, Yu Zhang<sup>a</sup>,  
Jun-Qing Wang<sup>a</sup>, Xiao-Fei Chen<sup>a</sup>

<sup>a</sup> China Nuclear Industry Survey Design & Research Co., Ltd., Zhengzhou 450000, China

<sup>b</sup> Hunan Provincial Engineering Research Center for Advanced Technology and Intelligent Equipment for Underground Space Development, Hunan University, Changsha 410082, China

<sup>c</sup> College of Civil Engineering, Hunan University, Changsha 410082, China

Received 31 October 2024; received in revised form 13 March 2025; accepted 1 April 2025

Available online 9 July 2025

## Abstract

The soil arching effect induced by deep-buried shield tunneling strongly influenced the ground stress and displacement. Therefore, revealing the evolution mechanism of the soil arching effect is a prerequisite for accurately predicting the tunnel load, which has not been understood in deep-buried conditions. Three model tests and eight numerical simulations were carried out to enhance the understanding of the soil arching evolution, in which the stress field, displacement field, and strain field were analysed. The experimental and numerical results indicated that the ground reaction curve presented a two-stage development process of an initially linear decrease followed by a gradual decrease. Compared with the theoretical tunnel loads, the measured and numerical values are relatively larger due to the loosening earth pressure theory ignoring the evolution process of the soil arching effect. The soil arching height decreases with the increase in stress level, measuring  $1.75D$  (the initial diameter of the model tunnel),  $1.65D$ , and  $1.61D$ , respectively, which results from the lagging evolution of the soil arching effect under high-stress conditions. The formation of the shear band was affected by the stress-dependent dilatancy of the soil. At low stress levels, the shear band develops vertically upward. In contrast, at higher stress levels, the shear bands tilt towards the lateral side.

**Keywords:** Soil arching effect; Ground reaction curve; Model test; Numerical simulation; Deep-buried shield tunnel

## 1 Introduction

With urban development, the utilization of shallow underground space has become saturated. Exploring the development of the deep underground space is now urgently needed. Deep-buried shield tunnels are one of the most important alternatives (Jiang et al., 2011; Liu et al., 2014; Li et al., 2023; Song et al., 2023a). Accurately determining the tunnel load is essential for the structural

design of the deep-buried tunnel, which is closely related to tunneling-induced soil arching effect (Evans, 1983; Rui et al., 2018; Burke & Elshafie, 2021b; Lin et al., 2021; Chen et al., 2022). However, the soil arching evolution mechanism in deep-buried shield tunneling is still not fully understood and further research is necessary.

Since Terzaghi (1943) carried out trapdoor tests and proposed the loosening earth pressure theory, more scholars conducted numerous experimental tests (Adachi et al., 2003; Jacobsz, 2016; Franza et al., 2019; Khatami et al., 2019, 2020, 2021b; Burke & Elshafie, 2021a) and theoretical studies (Evans, 1983; Zhang et al., 2016; Wu et al., 2019; Liang et al., 2020; F. Chen et al., 2025) to study the tunneling-induced soil arching effect. According to a series

\* Corresponding author at: College of Civil Engineering, Hunan University, Changsha 410082, China.

E-mail address: [chenrp@hnu.edu.cn](mailto:chenrp@hnu.edu.cn) (R.-P. Chen).

Peer review under the responsibility of Tongji University

of centrifugal tunnel excavation model tests, Lee et al. (2006) studied the soil arching evolution and proposed stress-related determination methods of the outer boundary of the soil arching zone. Liang et al. (2020) conducted the classic trapdoor tests and obtained the relationship between the evolution of the shear band and the ground reaction curve (GRC). Based on the experimental results, the arching theory for predicting the minimum and the residual values on the trapdoor was promoted. Franza et al. (2019) analyzed changes in overburden pressure and shear strain variations obtained by experimental tunneling model tests, detailing the evolution process of the soil arching effect with different soil relative densities and cover depths. In addition to the abovementioned research, numerical simulations were widely employed to simulate tunneling processes, serving as an important complement to model tests and enriching the experimental data that are difficult to measure (Khatami et al., 2021a; Xiong et al., 2023, 2024; Chen et al., 2024). Chen et al. (2011) established the three-dimensional numerical model and offered insight into the progressive development of the soil arching effect following step-by-step tunneling. Jiang and Yin (2012) investigated the stress redistribution around the tunnel induced by tunneling using the discrete element method (DEM) and the soil arching and unloading effects were discussed. Through trapdoor tests and numerical modeling, Chevalier et al. (2012) studied the load transfer mechanism with the increase in trapdoor displacement and observed the maximum arching phase, load recovery phase, and ultimate arching phase in the ground reaction curve. Khatami et al. (2021a) investigated the onset and evolution of the soil arching effect using DEM indicating that a stable arch forms when the particle size is large relative to the trapdoor width.

Although extensive experimental and numerical simulation studies have been conducted on the inner mechanism of the tunneling-induced soil arching effect, existing research has the following problems: (1) The trapdoor tests were widely utilized, however, the resulting ground displacement pattern is different from the actual engineering. (2) The stress levels were relatively low and the stress environment of the deep-buried tunnel can not be truly considered. (3) The effect of soil mechanical characteristics on the soil arching evolution has not been studied clearly.

In this study, the deep-buried shield tunneling model tests are first introduced. Then, to enrich the experimental data and further investigate the soil arching effect induced by deep-buried shield tunneling, a series of numerical models were established based on the model tests. The variation of earth pressure, soil displacement, and shear strain was analyzed. Comparisons between the measured data and the numerical results were carried out to verify the rationality of the numerical model. Subsequently, the effect of soil dilatancy on the soil arching effect was discussed. Finally, the development law of the ground reaction curve and the shear band was presented revealing the evolution mechanism of the soil arching effect induced by deep-buried shield tunneling.

## 2 Laboratory model test

### 2.1 Experimental program and setup

As shown in Fig. 1, to investigate the soil arching effect induced by deep-buried tunnel excavation, the model box, loading device, and mechanical contraction device (i.e., model tunnel) were employed to conduct the plane-strain model test of deep-buried shield tunnel excavation. Vertical stress on the top of the soil ( $p_s$ ) is applied through the loading device. The ground loss induced by tunnel excavation is simulated by adopting the mechanical contraction device.

The internal dimensions of the model box are 1000 mm in length, 1000 mm in width, and 1250 mm in depth. A 600 mm × 900 mm tempered glass is installed in front of the model box to capture the soil movement. The maximum output load of the servo actuator is 1000 kN, exerting a maximum pressure of 1.0 MPa. The model tunnel, with an initial diameter of 250 mm, is installed in the model box. The ground loss induced by tunneling is simulated through the contraction of the model tunnel, whose diameter variation is conducted by the horizontal telescopic rod driving the conical lock core along the internal axis (Fig. 1 (b)). The movement of the horizontal telescopic rod is driven by the manual bidirectional hydraulic pump. The distance between the bottom of the model tunnel and the inner surface of the bottom of the model box is 250 mm. The variation range of the model tunnel is 250–239.8 mm. The ground loss ratio ( $\eta$ ) of the tunnel is

$$\eta = \frac{V_L}{\frac{\pi D^2}{4}} = \frac{\frac{\pi D^2}{4} - \frac{\pi D_1^2}{4}}{\frac{\pi D^2}{4}} = 1 - \left(\frac{D_1}{D}\right)^2, \quad (1)$$

where  $V_L$  is the ground loss volume,  $D$  is the initial diameter of the model tunnel, and  $D_1$  is the diameter after the tunnel contracting. Therefore, the simulated ground loss ratio of the model tunnel is 0–8.0%.

To capture the change in earth pressure and ground movement, the pressure cells and the digital image correlation (DIC) testing system were employed in the experiments. The layout of the pressure cells can be seen in Fig. 2. To accurately measure the tunnel load variation, eight pressure cells were embedded around the model tunnel.

### 2.2 Testing material

According to the research of Tiwari et al. (2020) and existing geological data, the deep sand layer between 40 and 100 m in Shanghai is layer 9, which has the characteristics of small particle size (the median grain size  $D_{50}$  is 0.2 mm) and strong dilatancy (Fig. 3). Based on the distribution curve of the sandy soil layer 9 in Shanghai, the dry Fujian standard sand is used to prepare the soil sample of the model test. The basic parameters obtained by laboratory tests can be seen in Table 1 based on the direct shear

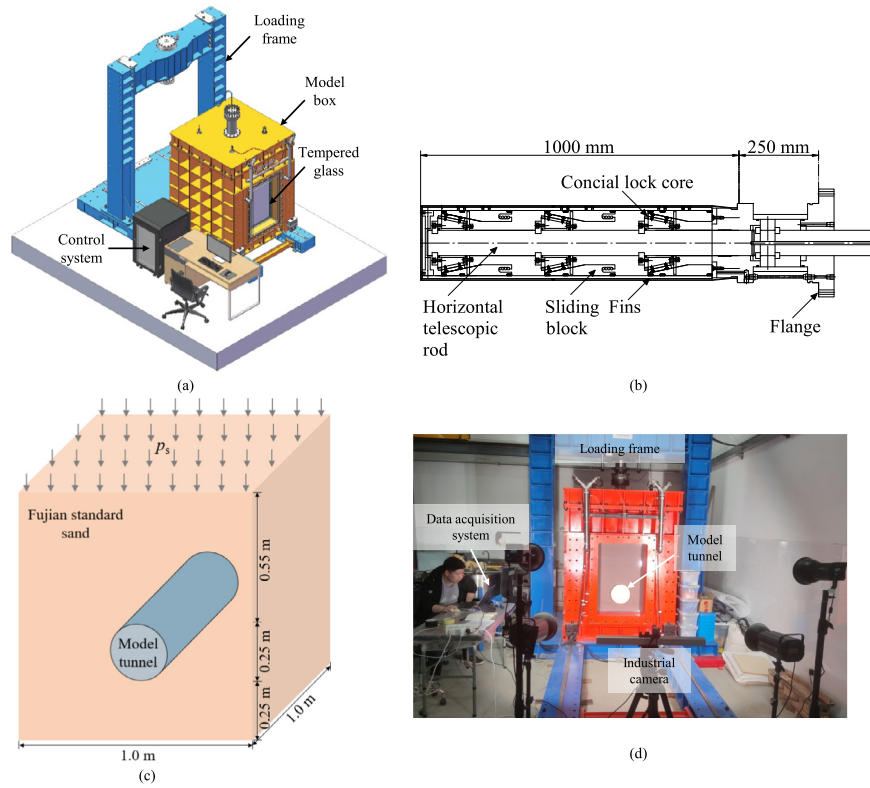


Fig. 1. Setup of the model tests (R. Chen et al., 2025): (a) model box and loading device, (b) mechanical contraction device, (c) schematic diagram, and (d) scene picture.

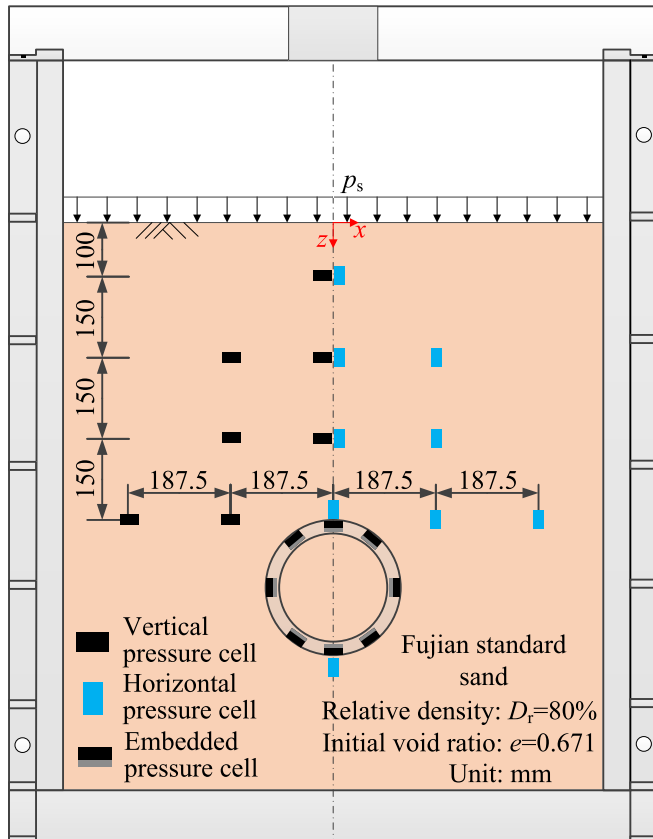


Fig. 2. Configuration of model tests.

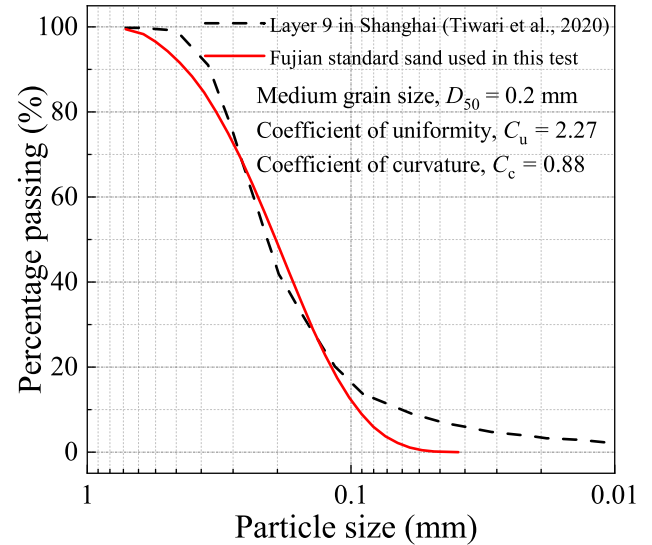


Fig. 3. Particle size distribution curve of Fujian standard sand.

Table 1  
Physical properties of the Fujian standard sand.

Material	$c$ (kPa)	$\phi$ ( $^\circ$ )	$G_s$	$\gamma_d$ (kN/m <sup>3</sup> )	$e$
Fujian standard sand	0	34	2.64	15.77	0.671

Note:  $c$  is the cohesion;  $\phi$  is the internal friction angle;  $G_s$  is the specific gravity;  $\gamma_d$  is the dry unit weight when the soil relative density is 80%;  $e$  is the initial void ratio when the soil relative density is 80%.

test, specific gravity test, and relative density test in the Standard for geotechnical testing method (Ministry of Water Resources of the People's Republic of China, 2019). Moreover, the consolidated drained triaxial tests were conducted with the confining pressures of 150, 450, and 800 kPa (Fig. 4). The results presented that the peak dilatancy angle ( $\psi_{\max}$ ) decreases with the increase of confining pressure, indicating that soil dilatancy decreases with the increase of the stress level, which is consistent with the conclusion of the existing research (Bolton, 1986; Schanz & Vermeer, 1996; Cincicoglu & Abadkon, 2015). The model test was carried out at the same relative density of 80%, with a unit weight of 15.77 kN/m<sup>3</sup> and an initial void ratio of 0.671. The dry pluviation method combined with the layer-by-layer method was adopted in the preparation of soil samples.

### 2.3 Scaling relation

Altaee and Fellenius (1994) proposed a set of scaling relations for 1g (gravity) model tests to determine the void ratio of sand. The scaling relations are shown in Table 2. Experiments were conducted under the stress applied to the upper soil, which can be considered that the stress level at the model tunnel crown is equal to that of the prototype (i.e., the stress similarity ratio  $N = 1$ ). Thus,  $e_m = e_p$ , indicating that the gradation and void ratio of the prototype soil and test soil can remain consistent. The diameter of the model tunnel in this study is 0.25 m (i.e., the geometric similarity ratio  $n = 1$ ), rather than a large-diameter tunnel. In this case, although it cannot simulate the excavation of large-diameter tunnels, it can serve as a preliminary exploration of the response of deep-buried shield tunneling. After parameter normalization, some instructive results can also be obtained.

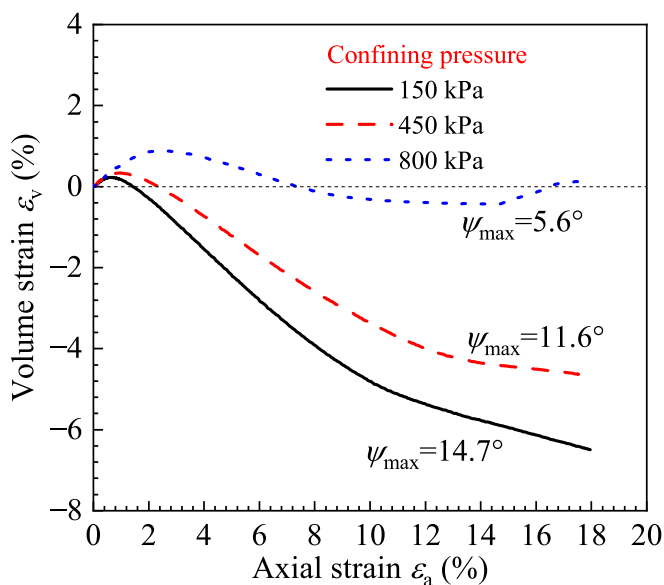


Fig. 4. Results of triaxial tests (R. Chen et al., 2025).

### 2.4 Test arrangement

In the experiments, the stress level with different cover depths was mainly considered. The distance between the fill surface and the tunnel crown is 0.55 m. The different stress levels exerted through the loading device, with the different vertical stress ( $p_s$  in the Fig. 1(c)) acting on the top of the soil. The stress values are 149.0 ( $=15.77 \times (10-0.55)$ ), which is determined by subtracting the self-weight of the upper fill of the model tunnel from the vertical stress of the soil at the simulated tunnel cover depth), 464.4, and 779.8 kPa, and corresponding simulated cover depths of dry sand ground are 10, 30, and 50 m, respectively (Table 3).

## 3 Numerical simulation

### 3.1 Numerical model

According to the setup of model tests, the two-dimensional finite element model (FEM), as can be seen in Fig. 5, was established to further investigate the soil arching evolution induced by deep-buried shield tunneling and the effect of soil dilatancy on the soil arching effect adopting the software of PLAXIS 2D 2024.1.0. The dimensions of the numerical model are 1000 mm (width)  $\times$  1050 mm (depth). To ensure the consistency of the numerical simulation and model test, loading pressure, with the same value as the model test, is applied on the top of the ground to simulate the stress environment of the deep-buried shield tunnel. The 15-node triangular elements were employed to model the soil mass, with a total of 21 015 nodes and 2573 elements. As for the displacement boundary condition, the normal direction of two lateral boundaries was fixed and the bottom boundary was fully fixed in both horizontal and vertical directions. In addition to this, the top boundary of the numerical model was set to displace freely.

The model tunnel is simulated using the plate elements, with an initial diameter of 250 mm. The tunnel contraction function in the finite element software was employed to simulate the tunneling-induced ground loss with the ground loss ratio of 0–8.0%, whose tunneling process is consistent with the model test. To sum up, the model size, loading pressure value, boundary condition, and tunneling process in the numerical model are all consistent with the model tests. Thus, the rationality of the numerical model can be verified by employing the measured data in model tests and further research on the soil arching effect induced by tunneling can be conducted using the FEM to reduce the expenses.

### 3.2 Analysis case

As can be seen in Table 4, based on the model tests, eight numerical models were established with different loading pressure ( $p_s$ ), peak dilatancy angle ( $\psi_{\max}$ ), and the coefficient of lateral earth pressure at rest ( $K_0$ ) to fur-

Table 2  
Scaling relations of the physical modeling approach (Altaee & Fellenius, 1994).

Scale	Linear dimension	Acceleration	Stress	Strain	Displacement	Force	Void ratio
Prototype	1	1	1	1	1	1	$e_p$
Model	$n$	1	$N$	1	$n$	$Nn^2$	$e_m = e_p + \lambda \ln N$

Note:  $n$  is the geometric similarity ratio;  $N$  is the stress similarity ratio;  $e_p$  is the void ratio of the prototype soil;  $e_m$  is the void ratio of the test soil;  $\lambda$  is the slope of the steady line in  $e$ - $\ln p$  plane.

Table 3  
Test arrangement.

Case	$p_s$ (kPa)	$H$ (m)
1	149.0	10
2	464.4	30
3	779.8	50

Note:  $p_s$  is the loading pressure acting on the top of the soil;  $H$  is the simulated cover depth.

Table 4  
Analysis case.

Case	$p_s$ (kPa)	$H$ (m)	$\varphi$ (°)	$\psi_{max}$ (°)	$K_0$
1	149.0	10	34	14.7	0.51
2	464.4	30	34	11.6	0.58
3	779.8	50	34	5.6	0.59
4	0	0.55	34	14.7	$1 - \sin\varphi = 0.44$
5	779.8	50	34	0	0.59
6	779.8	50	34	$0.3\varphi$	0.59
7	779.8	50	34	$0.5\varphi$	0.59
8	779.8	50	34	$1.0\varphi$	0.59

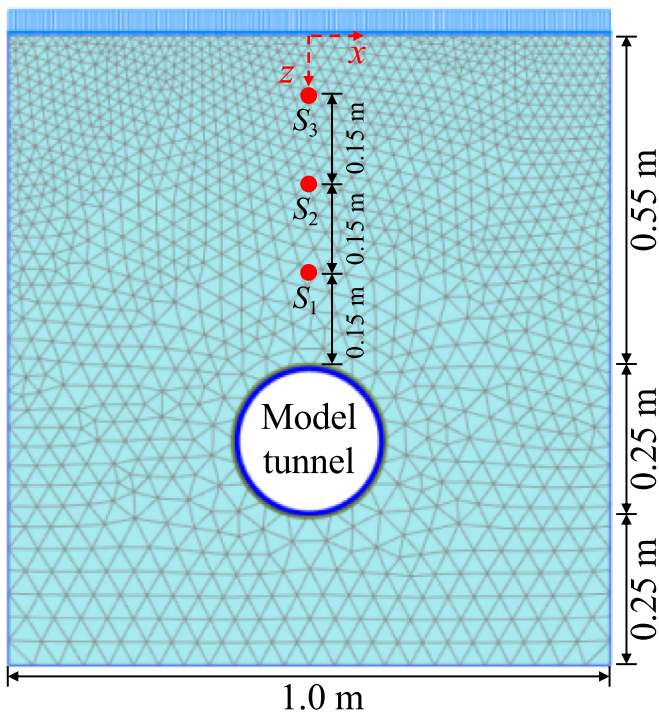


Fig. 5. Numerical model.

ther investigate the soil arching effect induced by deep-buried shield tunneling. Other parameters, like internal friction angle ( $\varphi = 34^\circ$ ) and relative density ( $D_r = 80\%$ ,  $\gamma_d = 15.77 \text{ kN/m}^3$ ,  $e = 0.671$ ), remain unchanged. Cases 1–3 were set up to reproduce the aforementioned model tests to obtain some results that are difficult to measure (such as the range of the arching zone and the stratified settlement). Besides, the measured data obtained from model tests can be used to verify the rationality of the numerical simulation. The  $\psi_{max}$  values were obtained by triaxial tests (Fig. 4). The coefficient of lateral earth pressure at rest val-

ues were set to be equal to the average measured values of model tests. Case 4 was set up to simulate the shallow-buried tunneling just like a control group in an experiment, which can be used to compare the evolution difference of soil arching effect induced by deep-buried and shallow-buried shield tunneling. According to laboratory tests, Bolton (1986) studied the dilatancy of sand with different stress levels and found that soil dilatancy was not affected by the stress level change when the mean effective stress is less than 150 kPa. Therefore, the  $\psi_{max}$  value was set to be equal to that of Case 1. The coefficient of lateral earth pressure at rest value was set to be equal to  $1 - \sin\varphi$ . Cases 5–8 were set up to investigate the effect of a single factor of soil dilatancy on the soil arching evolution. The  $\psi_{max}$  values were set as 0,  $0.3\varphi$ ,  $0.5\varphi$ , and  $1.0\varphi$ , respectively. Other parameters remained unchanged, and values were set to be equal to those of Case 3.

### 3.3 Material models and parameters

The interface element between the soil and the model tunnel is established, however, without consideration of the strength reduction (i.e.,  $R_{int} = 1.0$ ). As can be seen in Table 5, an advanced constitutive model namely the Hardening soil model with Small Stiffness (HSS) was adopted to cope with the stress–strain behavior of Fujian standard sand. The HSS model was developed with the consideration for the small strain characteristics of soil. Its advantages are as follows: (1) It is well-suited for dealing with the tunneling-induced stress–strain relationship of soil across both small and large strain ranges. (2) It assumes that the elastic modulus is stress-dependent, allowing for simulations that investigate the effect of stress level on soil arching evolution. (3) The parameters can be easily

Table 5  
Parameters of the HSS model.

Parameters		Value	Unit
$\gamma$	Unit weight	15.77	kN/m <sup>3</sup>
$E_{50}^{\text{ref}}$	Reference secant stiffness in triaxial test	16 280	kN/m <sup>2</sup>
$E_{\text{oed}}^{\text{ref}}$	Reference tangent stiffness for oedometer loading	12 930	kN/m <sup>2</sup>
$E_{\text{ur}}^{\text{ref}}$	Reference unloading/reloading stiffness	74 290	kN/m <sup>2</sup>
$m$	Power that controls the stress dependency of stiffness	0.7	–
$c'_{\text{ref}}$	Effective cohesion	0	kN/m <sup>2</sup>
$\phi'$	Effective friction angle	34	(°)
$\psi$	Dilatancy angle	See Table 4	(°)
$\gamma_{0.7}$	Shear strain at which $G_s = 0.772G_0$	$3.9 \times 10^{-4}$	–
$G_0^{\text{ref}}$	Reference shear modulus at very small strains ( $\epsilon < 10^{-6}$ )	118 400	kN/m <sup>2</sup>
$\nu'_{\text{ur}}$	Poisson's ratio of unloading/reloading	0.2	–
$p^{\text{ref}}$	Reference stress	100	kN/m <sup>2</sup>
$R_f$	Failure ratio	0.9	–
$e_0$	Initial void ratio	0.671	–
$e_{\text{min}}$	Minimum void ratio	0.603	–
$e_{\text{max}}$	Maximum void ratio	0.944	–
$K_0$	The coefficient of lateral earth pressure at rest	See Table 4	–

obtained based on existing research. Meanwhile, the HSS model also has several limitations, as it requires a large number of input parameters, which may increase the workload for both calculations and experiments. Gu et al. (2021) proposed the determination method between the main parameters of the HSS model of Shanghai soil and mechanical properties based on a large number of laboratory and field test data. The main parameters of the HSS model in this study were determined utilizing this empirical method. The dilatancy angle and the coefficient of lateral earth pressure at rest values can be seen in Table 4, in which the  $\psi_{\text{max}}$  values of Cases 1–4 are determined by triaxial test results in Section 2.2. The model tunnel was regarded as the linear elasticity material with Young's modulus and Poisson's ratio of 230 GPa and 0.3, respectively (Table 6).

## 4 Results

### 4.1 Variation of earth pressure

#### 4.1.1 Variation of earth pressure on tunnel crown

The variation in vertical stress on the tunnel crown with the ground loss ratio is generally called the ground reaction curve. It has great significance to reflect the evolution process of the soil arching. In this study,  $p$  is the corresponding vertical/horizontal stress with a certain ground loss ratio and  $p_0$  is the initial vertical/horizontal stress.

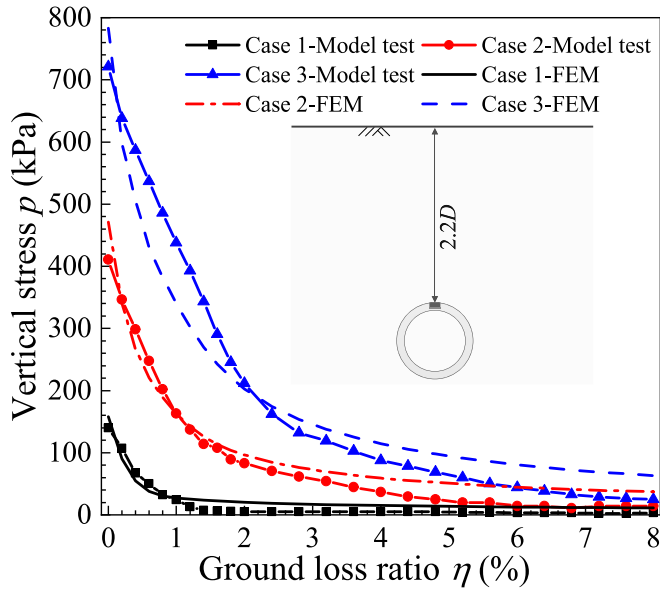
Figure 6 shows the GRCs obtained by model tests and numerical simulations. The two stages of development of

GRCs induced by tunneling are found: (1) linear rapid decreasing stage in vertical stress; (2) gradual decreasing stage in vertical stress. The variation trend is similar to the result of the centrifugal tunnel excavation model tests of Franza et al. (2019). As can be seen in Fig. 6(b), the slope of the linear rapid decrease stage decreases with the increase in stress level, indicating the slower development of soil arching in the deep-buried condition. It can be inferred that the deeper the cover depth, the lower the soil arching height. Therefore, in the same ground loss, the deep-buried tunnel excavation corresponds to the larger overburden pressure compared with the shallow-buried condition. The ultimate soil arching ratio values with different stress levels are relatively close, showing that the soil arching ratio in the critical state is independent of the stress level. In addition, the numerical results align well with the experimental results, both in terms of the overall trend and the concrete values, thereby validating the rationality of the numerical model.

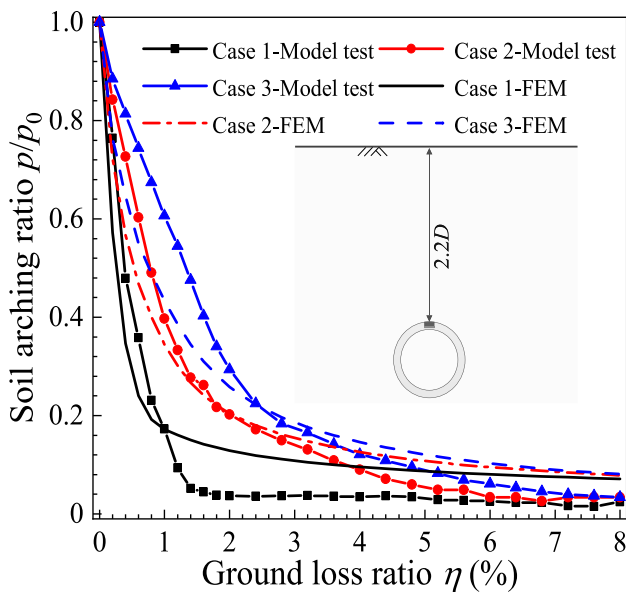
Figure 7 presents the variation in horizontal stress induced by tunneling. The horizontal stresses on the tunnel crown first increase to the maximum value and then gradually decrease with the increase in the ground loss ratio. The reason is that the tunneling-induced soil arching effect results in the vertical stress transferring to the horizontal direction in the early stage, leading to an increase in horizontal stress. Besides, the arching-induced increase in horizontal stress is greater than the unloading-induced decrease in horizontal stress. The ground loss ratio value corresponding to the maximum stress increases with the increase in the stress level, which also indicates the slower development of soil arching in the deep-buried condition. Compared with the model test results, the numerical results show the same trend, but the specific values are different, which may be caused by the deflection of the sensor in the experiment process.

Table 6  
Material parameters of the model tunnel.

Material model	Young's modulus $E$ (GPa)	Poisson's ratio $\nu$
Linear elasticity	230	0.3



(a)



(b)

Fig. 6. Variation of the GRC at tunnel crown: (a) vertical stress, and (b) normalized vertical stress.

4.1.2 Variation of the earth pressure around the tunnel

Figure 8 shows the normalized vertical/horizontal stress around the tunnel with a ground loss ratio of 1.0%. The numerical results, measured values, and theoretical values are compared.  $r_{sa}$  is the soil arching ratio representing the normalized vertical stress on the tunnel crown.  $N_c$  is the normalized horizontal stress on the tunnel crown.  $N_w$  is the normalized horizontal stress at the tunnel waist.  $N_b$  is the normalized horizontal stress at the bottom of the

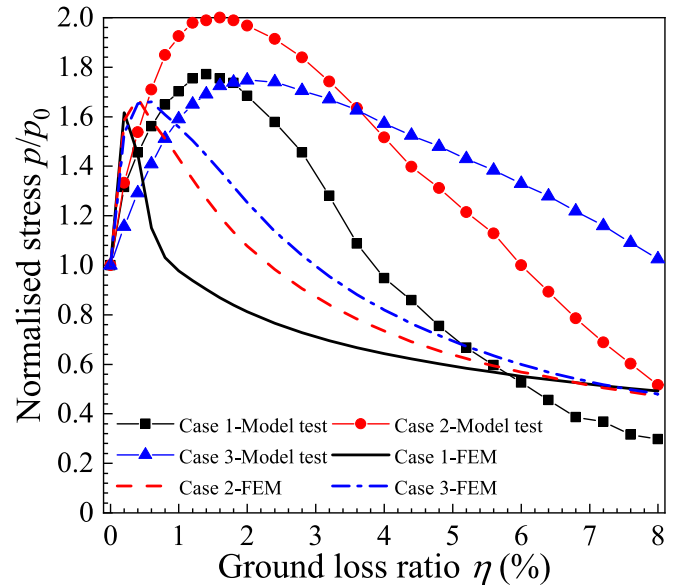


Fig. 7. Variation of the horizontal stress at the tunnel crown.

tunnel. The theoretical values calculated by the Chinese standard for design of shield tunnel engineering (Ministry of Housing and Urban-Rural Development of the People’s Republic of China, 2021). In the standard, the vertical stress on the tunnel crown (overburden pressure) is calculated by Terzaghi’s loosening earth pressure theory. The horizontal stress is obtained by multiplying the sum of the overburden pressure and the self-weight stress of the soil from the calculated position to the tunnel crown by the coefficient of lateral earth pressure at rest. Thus, the lateral horizontal stress is highly correlated with the overburden pressure in the standard.

Overall, the numerical results are close to the measured values obtained by model tests, which further verifies the rationality of the numerical model. Compared with the measured and numerical results, the theoretical tunnel loads are much smaller, and the larger the stress level, the greater the difference. This is due to Terzaghi’s theory ignoring the effect of the construction process (i.e., the development process of the soil arching effect), and the soil arching effect was considered in the critical state. However, the soil arching evolution is a gradual development process (Fig. 6). When  $\eta = 1.0\%$ , the soil arching effect is in the initial linear decrease stage resulting in the abovementioned difference. For the  $N_c$ , compared with the theoretical values, the results obtained by FEM and model test are significantly larger, which is due to the initial increase of the horizontal stress caused by the tunneling-induced soil arching effect (Fig. 8). However, the theoretical method ignored this phenomenon. For the  $N_w$ , it can be seen that its magnitude increases with the increase of stress level in the FEM and model test and its magnitude is smaller than the  $N_c$  and  $N_b$  due to the stronger unloading. For the  $N_b$ , it can also be seen that it is close to the initial value, which does not seem to be affected by the excavation unloading. The truth is that the horizontal stress at the bottom of the tunnel ( $N_b$ )

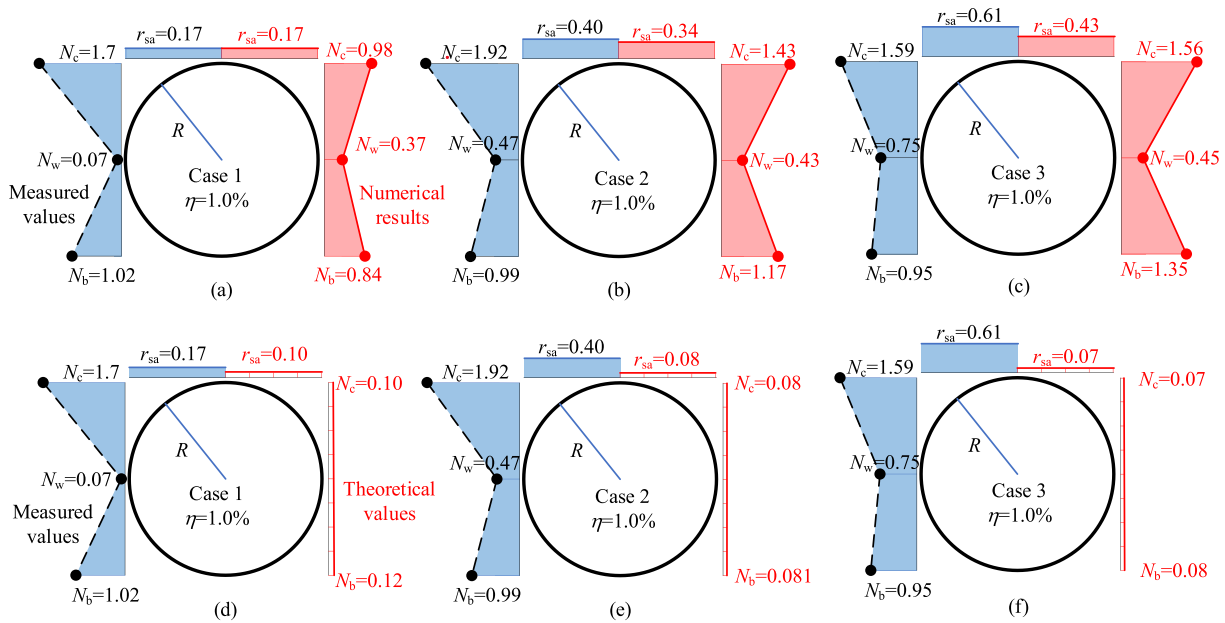


Fig. 8. Normalized stress around the tunnel.

also went through the initial increase stage like the  $N_c$  (Fig. 8), resulting in the larger stress value in the condition of  $\eta = 1.0\%$ .

As the ground loss ratio increases from 1.0% to 8.0%, the numerical and measured results will be closer to the theoretical values due to the gradual development of the soil arching effect. However, the practical engineering tunneling-induced ground loss ratio is between 0.02% and 3.36% (Wu & Zhu, 2018), which will result in larger actual tunnel loads than the predicted values obtained by Terzaghi's theory. It should be carefully noticed in the structural design.

#### 4.1.3 Variation of the earth pressure above the tunnel

Figure 9 shows the changes in two-dimensional stress at three given points ( $S_1$ ,  $S_2$ , and  $S_3$  in Fig. 5) during the excavation process. On the whole, it can be seen that the vertical stress decreases with the increase in the ground loss ratio, and the horizontal stress increases with the increase of ground loss ratio presenting the typical characteristics of stress redistribution in the soil arching evolution process. In every case, the closer the distance between the stress point and the model tunnel, the greater the decrement in the vertical stress due to the stronger unloading soil arching effect.

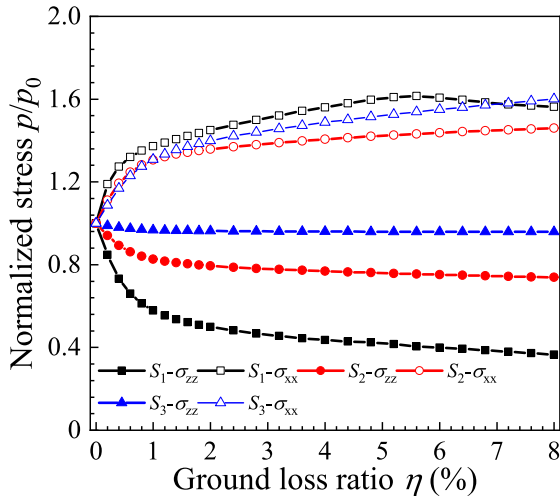
Compared with Case 1, the variation process in Cases 2 and 3 is basically the same due to the higher stress level. The stress change is more significant in the condition of relatively low stress (Case 1), indicating the stronger soil arching effect in the condition of the low stress level compared with the other two conditions of the higher stress level (Cases 2 and 3). A significant decrease in horizontal stress occurred in point  $S_1$  of Case 1 when the ground loss ratio exceeded 6%, indicating that the unloading-induced reduc-

tion in horizontal stress outweighs the increase caused by soil arching. It also shows that the tunneling-induced influence height is larger under conditions of low stress levels. Thus, the larger range of the soil arching effect may form in the condition of low stress level.

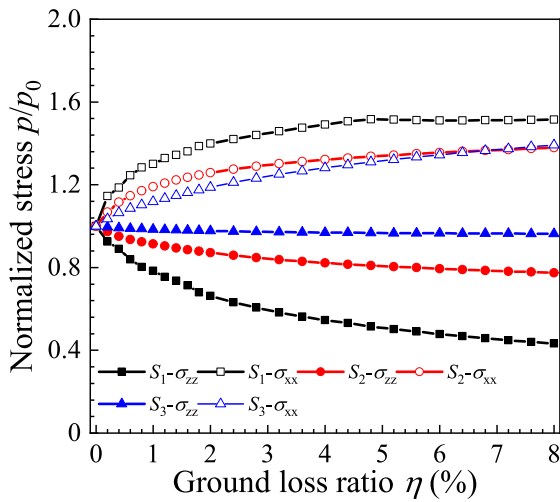
#### 4.1.4 Variation of the soil arching zone induced by tunneling

To determine the scope of the soil arching zone, the determination method according to the change of vertical stress proposed by Song et al. (2023b) was adopted here. The variations in ground vertical stress obtained by FEM are analyzed, which are difficult to obtain in experimental tests. Figure 10 shows the distribution of the outer boundary of the soil arching zone drawn by this determination method induced by tunneling when the ground loss ratio is 3.2%. It can be seen from the figure that the soil arching height decreases with the increase of the stress level, which is  $1.75D$ ,  $1.65D$ , and  $1.61D$ , respectively. In addition, the lateral range of the soil arching effect decreases with the increase of the stress level. The phenomenon can correspond to the abovementioned deduction of “the deeper the cover depth, the lower the soil arching height” (Section 4.1.1) and “the larger range of the soil arching effect may form in the condition of low stress level (see Section 4.1.3)”. This is the result of the abovementioned lagging evolution of the soil arching effect in the condition of high stress level (deep-buried condition).

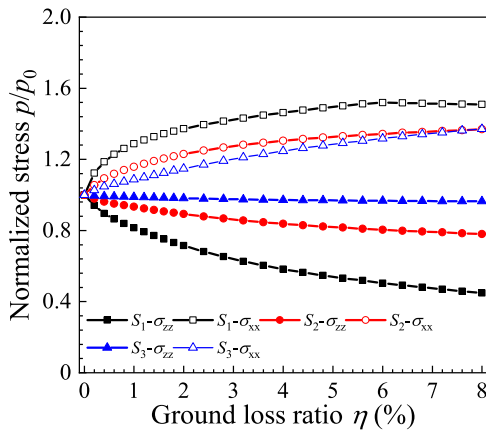
To further investigate the reason for the scope variation of the soil arching zone with different stress levels, the development of the ground settlement at the top elevation of the tunnel with different ground loss ratios was presented here (Fig. 11). In Fig. 11, the ground settlement is  $v/D$  ( $v$  is ground settlement) and the differential settlement is  $\Delta$ , which is equal to the settlement difference between the



(a)



(b)



(c)

Fig. 9. Variation of the earth pressure above the tunnel: (a) Case 1-FEM, (b) Case 2-FEM, and (c) Case 3-FEM.

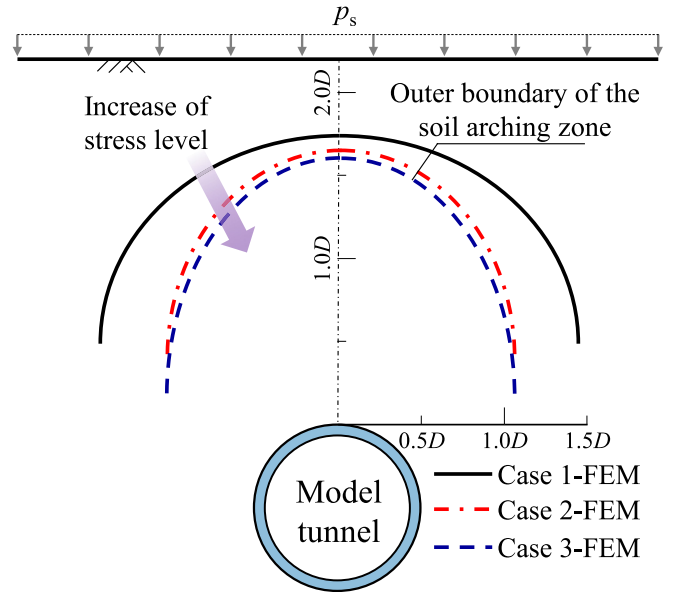


Fig. 10. Distribution of the outer boundary of the soil arching zone.

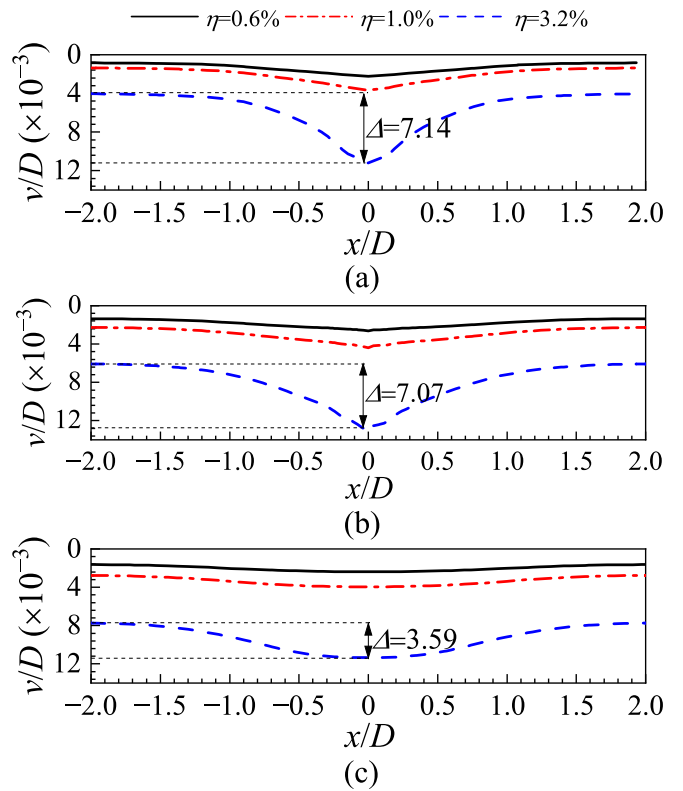


Fig. 11. Changes in the settlement at the top elevation of the tunnel: (a) Case 1-FEM, (b) Case 2-FEM, and (3) Case 3-FEM.

settlement on the tunnel centerline and the lateral boundary of the FEM. As an important factor inducing the soil arching effect, the differential settlement is closely related to the development of the soil arching effect. It can be seen

that the ground settlement and the differential settlement increase with the increase of the ground loss ratio. However, the differential settlement decreases with the increase in the stress level, which is the root reason why the soil arching effect develops slowly under the high stress level (deep-buried condition). In other words, with the increase in stress level, the differential settlement becomes smaller, resulting in the weakening of the soil arching effect, and the decrease of soil arching height and the lateral width.

#### 4.2 Variation of shear band induced by shield tunneling

Figure 12 shows the variation of the shear band induced by tunneling obtained by numerical simulation and model test. Overall, using the tunnel centerline as the reference, the starting points of the shear bands are located at the intersections of  $\pm 45^\circ$  radii and the tunnel perimeter. Only the development of the upper shear band is analyzed in detail due to its great impact on the overburden pressure. In Fig. 12(a), it can be seen that the development direction of the shear band is close to vertical under the condition of  $p_s = 0$  and  $\psi_{\max} = 14.7^\circ$ , however, it tilts towards both sides with the high stress level and weak soil peak dilatancy angle. In Fig. 12(b), the inclination degree increases with the increase of the stress level and the decrease of the soil peak dilatancy angle. As mentioned before, the soil dilatancy decreases with the increase in stress level (Section 2.2).

Therefore, it can be inferred that the decrease in soil dilatancy induced by the increase in the stress level results in the inclination of the shear band. To further study the effect of the single factor of the soil dilatancy on the development of the shear band, the numerical results of Cases 5 and 8 are adopted (Fig. 12(c)). It can be indicated that the inclination angle between the shear band and the horizontal direction decreases with the decrease of the soil peak dilatancy angle. That is also the reason why the soil arching height is low with the high stress level. The abovementioned phenomena can also be found in existing numerical simulations and model tests. Khalid et al. (2019) studied the effect of soil dilatancy on the shear band during tunneling and found that the inclination angle of the shear band increases with the increase of the dilatancy angle. Wong (1986) investigated the development of the shear band induced by tunneling at different cover depths. The research indicated that the inclination angle is  $75^\circ\text{--}90^\circ$  for shallow-buried conditions, while for deep-buried conditions, that is  $60^\circ\text{--}80^\circ$ . Moreover, the relative phenomena also were discovered in the centrifuge model tests of Franza et al. (2019). Hence, the relative deduction can be verified through numerical simulation and existing research.

Figure 12(d) and (e) shows the development process of the shear band obtained by FEM and model test. It can be seen that the development direction of the shear band

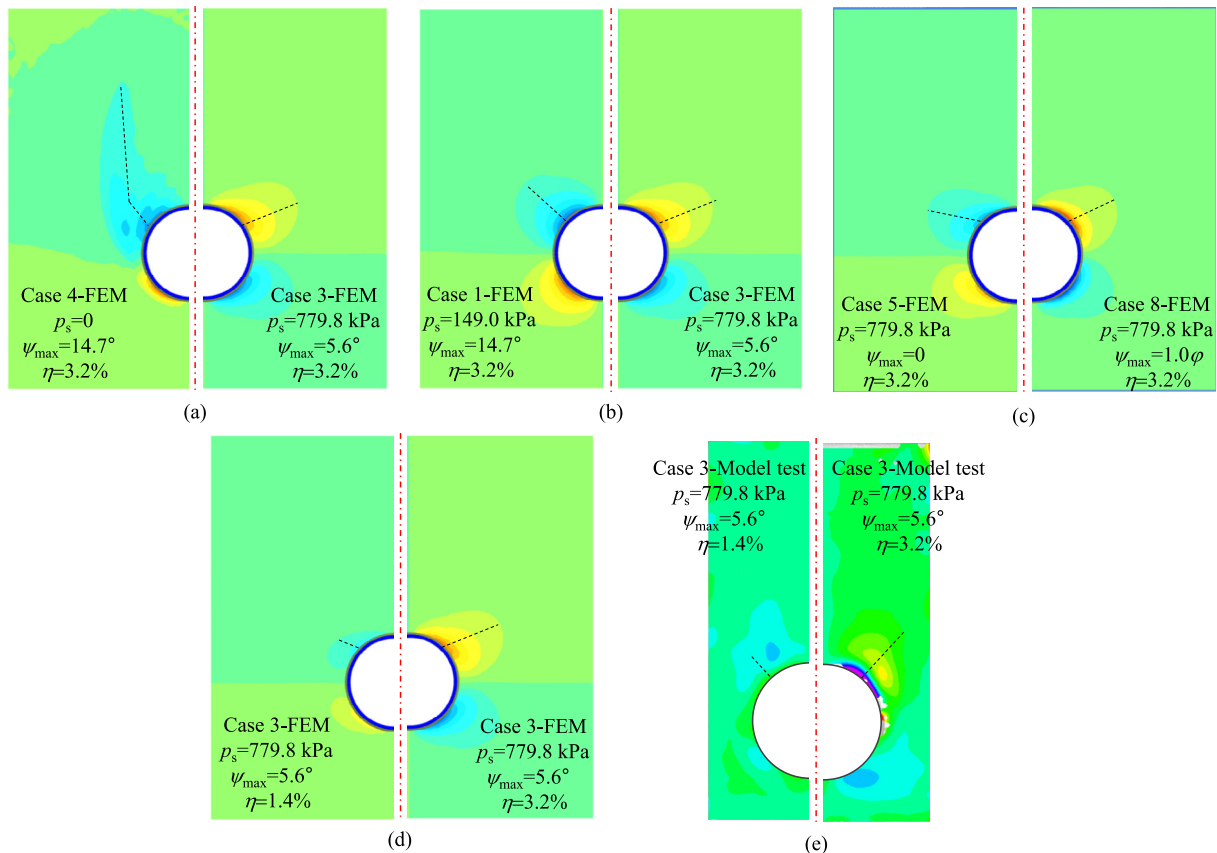


Fig. 12. Variation of shear band induced by shield tunneling.

remains unchanged as the increase of ground loss ratio, and the shear band extends upward along the initial direction. Additional experimental results can be seen in R. Chen et al. (2025).

Figure 13 shows the ground vertical deformation induced by tunneling under a ground loss ratio of 3.2%. As illustrated in the figure, the main deformation zone above the tunnel gradually expands laterally as the increase of stress level, which can correspond to the aforementioned tilted shear band due to stress-dependent soil dilatancy.

#### 4.3 Effect of dilatancy on soil arching effect

For the effect of the dilatancy on the shear band, as stated before, the inclination angle between the shear band and the horizontal direction decreases with the decrease of the soil dilatancy (Fig. 12(c)).

To assess the effect of dilatancy on stress redistribution, the changes in vertical and horizontal stress on the tunnel crown are analyzed under varying soil dilatancy (Fig. 14). As illustrated in Fig. 14(a), the GRCs all exhibit the aforementioned two-stage development characteristics (Section 4.1.1) under different soil dilatancy. The enhancement of dilatancy leads to an increased slope in the initial linear decreasing stage of the GRC, while the degree of stress reduction in the gradual decreasing stage is diminished, which is consistent with the results of the model tests of Franza et al. (2019). As can be seen in Fig. 14(b), the horizontal stress on the tunnel crown initially increases rapidly, reaching a maximum value when

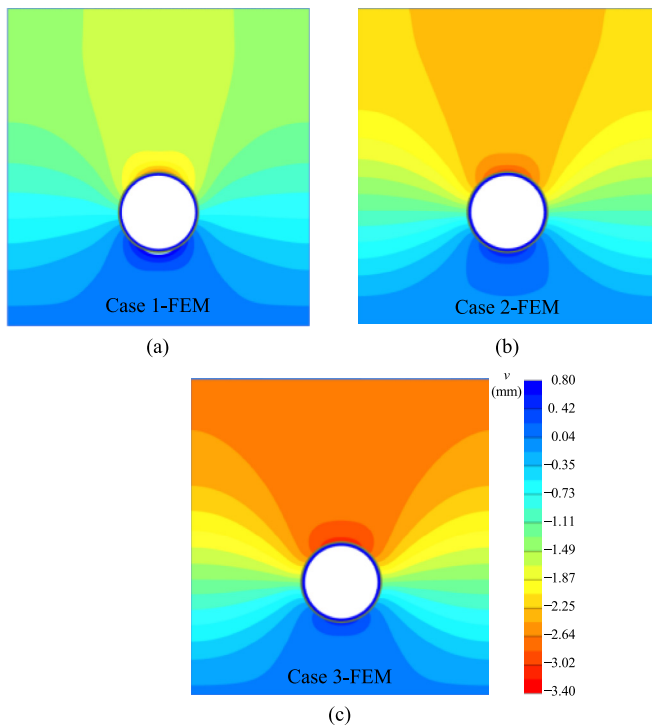
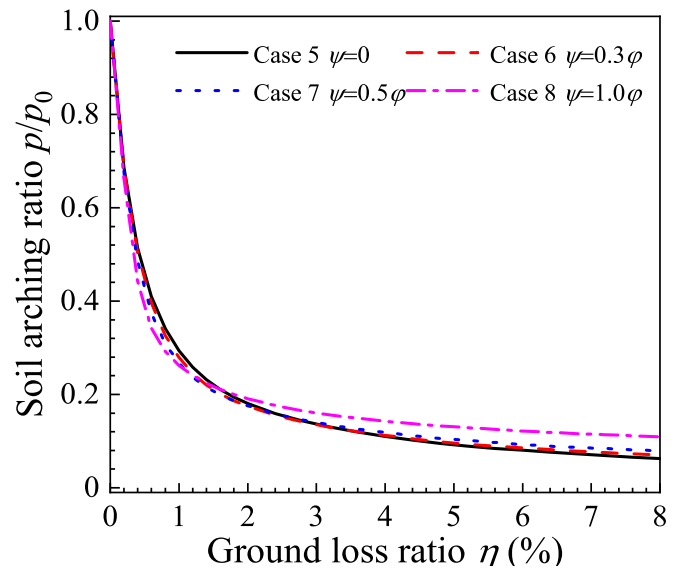
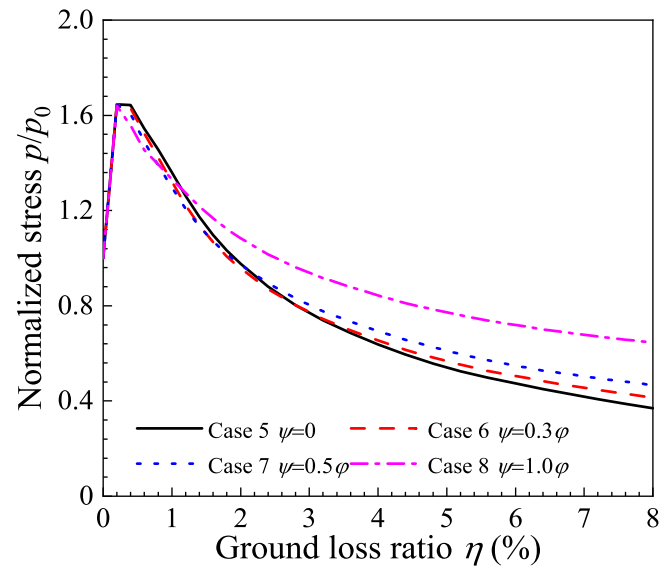


Fig. 13. Vertical deformation contour induced by tunneling: (a) Case 1-FEM, (b) Case 2-FEM, and (c) Case 3-FEM.



(a)



(b)

Fig. 14. Effect of soil dilatancy on stress variation at the tunnel crown: (a) normalized vertical stress, and (b) normalized horizontal stress.

the ground loss ratio is 0.2%. Subsequently, it decreases with the increase in the ground loss ratio, and the degree of stress reduction is also diminished as the enhancement of the soil dilatancy.

#### 4.4 Evolution mechanism of the soil arching effect

According to the previously presented understanding of the tunneling-induced soil arching effect obtained by model tests and numerical simulations, the schematic diagram illustrating the development of the GRC and the shear

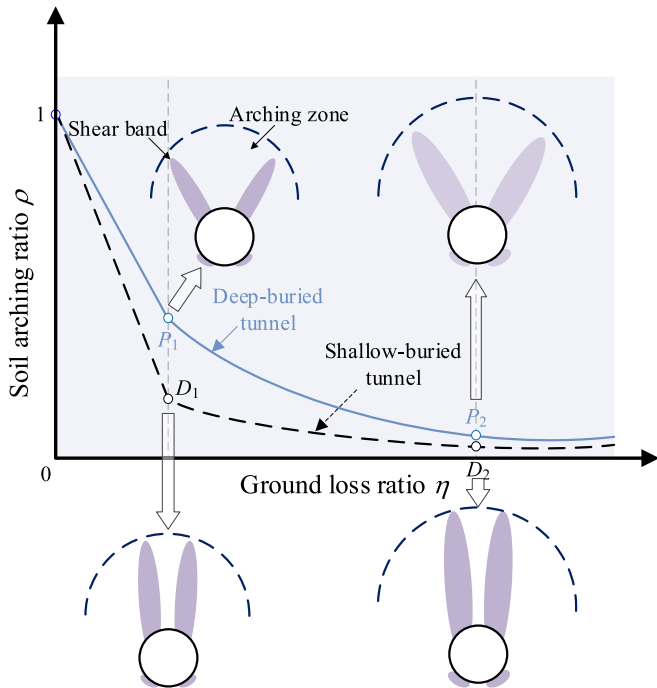


Fig. 15. Schematic diagram of the evolution of the soil arching effect induced by tunnel excavation.

band is shown (Fig. 15). The evolution process of the GRC and the shear band are concluded as follows:

For the GRC (Fig. 15), the two-stage development process of an initially linear decrease followed by a gradual decrease is categorized. As the stress level increases, the slope of the linear decrease stage of the GRC decreases indicating that the overburden pressure is larger in the high-stress level condition (deep-buried tunnel) under the same ground loss ratio compared with the low-stress level condition (shallow-buried tunnel).

For the shear band (Fig. 15), it is affected by the stress-dependent soil dilatancy. The shear band develops vertically upward under the very low-stress level (Case 4-FEM), whereas under the high-stress level, the shear band tilts towards the lateral side. Furthermore, once the shear band forms, its development direction remains unchanged despite the increasing ground loss ratio.

Through the above summary, a clearer understanding of the evolution mechanism of soil arching effect induced by deep-buried shield tunneling has been obtained, which can be used as a basis to propose the arching theory to more accurately determine the tunnel load.

## 5 Conclusions

Based on deep-buried shield tunneling model tests, eight numerical models were established to enrich experimental data and gain further insights into the tunneling-induced soil arching effect. By analyzing the stress field, displacement field, and strain field, the mechanism behind the development of the soil arching effect was revealed.

According to the results obtained by model tests and numerical simulations, the following conclusions can be summarized:

- (1) A two-stage development process of the GRC induced by tunneling was observed: (i) linear rapid decreasing stage; and (ii) gradual decreasing stage. The slope of the linear rapid decreasing stage reduces as the stress level increases, indicating a slower development of soil arching effect in the deep-buried condition. The ultimate soil arching ratio is independent of the stress level.
- (2) The outer boundary of the soil arching zone was determined by the changes in stress. The soil arching height decreases as the stress level increases, measuring  $1.75D$ ,  $1.65D$ , and  $1.61D$ , respectively, and so does the lateral range. This results from the lagging evolution of the soil arching effect under high-stress conditions.
- (3) The development of the shear band was influenced by the stress-dependent soil dilatancy. At a very low-stress level, the shear band develops vertically with stronger soil dilatancy. However, it tilts towards the lateral side at a high-stress level and weak soil dilatancy. The inclination of the shear band is caused by the increased stress-induced soil dilatancy weakening. Once the shear band forms, its development direction does not change with the increase in the ground loss ratio.
- (4) Based on the experimental and numerical results, the following issues need special attention in the future: (i) Further experimental and numerical research about tunnel excavation is required focusing on the influence of the tunneling process and tunneling parameters on the soil arching effect. (ii) The research on the effect of groundwater and seepage on the soil arching effect during shield tunneling is still needed. (iii) The theoretical model concerning the tunneling-induced arching effect should be established based on the experimental and numerical results of tunneling.

## Data availability

The data that support the findings of this study are available from the corresponding author upon reasonable request.

## CRediT authorship contribution statement

**Xu Song:** Investigation, Formal analysis, Validation, Writing – original draft. **Chang-Wei Miao:** Data curation, Resources. **Ren-Peng Chen:** Funding acquisition, Writing – review & editing, Conceptualization. **Xiao-Ning Deng:** Supervision. **Yu Zhang:** Methodology. **Jun-Qing Wang:** Visualization. **Xiao-Fei Chen:** Project administration.

## Declaration of competing interest

The authors declare that they have no known competing financial interests or personal relationships that could have appeared to influence the work reported in this paper.

## Acknowledgment

The research is supported by the National Natural Science Foundation of China (Grant Nos. 52090082 and 51938005).

## References

- Adachi, T., Kimura, M., & Kishida, K. (2003). Experimental study on the distribution of earth pressure and surface settlement through three-dimensional trapdoor tests. *Tunnelling and Underground Space Technology*, 18(2/3), 171–183.
- Altaee, A., & Fellenius, B. H. (1994). Physical modeling in sand. *Canadian Geotechnical Journal*, 31(3), 420–431.
- Bolton, M. D. (1986). The strength and dilatancy of sands. *Géotechnique*, 36(1), 65–78.
- Burke, T. S. D., & Elshafie, M. Z. E. B. (2021a). Arching in granular soils: Experimental observations of deformation mechanisms. *Géotechnique*, 71(10), 866–878.
- Burke, T. S. D., & Elshafie, M. Z. E. B. (2021b). Arching in granular soils: Limit state equilibrium. *Géotechnique*, 71(8), 700–713.
- Chen, C. N., Huang, W. Y., & Tseng, C. T. (2011). Stress redistribution and ground arch development during tunneling. *Tunnelling and Underground Space Technology*, 26(1), 228–235.
- Chen, F., Liu, X. H., Sun, J. F., Xiong, H., Yin, Z. Y., & Chen, X. S. (2025a). Micro mechanism and analytical model of stress distribution in loosened soil zone above active trapdoor. *Computers and Geotechnics*, 177, 106841.
- Chen, F. Q., Luo, S. C., & Lai, F. W. (2022). New analytical solutions for cohesive–frictional soils above deep active trapdoors. *International Journal of Geomechanics*, 22(12), 04022235.
- Chen, H. Q., Xiong, H., Qiu, Y. Y., Yin, Z. Y., & Chen, X. S. (2024). Catastrophic failure mechanism of underground complexes under deep construction disturbance. *Tunnelling and Underground Space Technology*, 154, 106059.
- Chen, R. P., Song, X., Meng, F. Y., Wang, H. L., Liu, Y., & Wen, L. (2025b). Experimental investigation on the soil arching effect induced by deep-buried shield tunneling. *Tunnelling and Underground Space Technology*, 155, 106161.
- Chevalier, B., Combe, G., & Villard, P. (2012). Experimental and discrete element modeling studies of the trapdoor problem: Influence of the macro-mechanical frictional parameters. *Acta Geotechnica*, 7(1), 15–39.
- Cinicioglu, O., & Abadkon, A. (2015). Dilatancy and friction angles based on in situ soil conditions. *Journal of Geotechnical and Geoenvironmental Engineering*, 141(4), 06014019.
- Evans, C. H. (1983). *An examination of arching in granular soils*. [Master dissertation, Massachusetts Institute of Technology, Cambridge].
- Franza, A., Marshall, A. M., & Zhou, B. (2019). Greenfield tunnelling in sands: The effects of soil density and relative depth. *Géotechnique*, 69(4), 297–307.
- Gu, X. Q., Wu, R. T., Liang, F. Y., & Gao, G. Y. (2021). On HSS model parameters for Shanghai soils with engineering verification. *Rock and Soil Mechanics*, 42(3), 833–845 (in Chinese).
- Jacobsz, S. W. (2016). Trapdoor experiments studying cavity propagation. In *Proceedings of 1st southern african geotechnical conference* (pp. 159–165). South Africa: Sun City.
- Jiang, M. J., & Yin, Z. Y. (2012). Analysis of stress redistribution in soil and earth pressure on tunnel lining using the discrete element method. *Tunnelling and Underground Space Technology*, 32, 251–259.
- Jiang, X. L., Li, L., Yuan, J., & Yin, J. S. (2011). Dynamic analysis of strata horizontal displacements induced by shield construction of deep tunnel. *Rock and Soil Mechanics*, 32(04), 1186–1192 (in Chinese).
- Khalid, M. S., Kikumoto, M., Cui, Y., & Kishida, K. (2019). The role of dilatancy in shallow overburden tunneling. *Underground Space*, 4(3), 181–200.
- Khatami, H., Deng, A., & Jaksa, M. (2019). An experimental study of the active arching effect in soil using the digital image correlation technique. *Computers and Geotechnics*, 108, 183–196.
- Khatami, H., Deng, A., & Jaksa, M. (2020). Passive arching in rubberized sand backfills. *Canadian Geotechnical Journal*, 57(4), 549–567.
- Khatami, H., Deng, A., & Jaksa, M. (2021a). Discrete element modelling of the trapdoor arching effect in sand and rubberised sand. *Proceedings of the Institution of Civil Engineers-Geotechnical Engineering*, 174(6), 657–669.
- Khatami, H., Deng, A., & Jaksa, M. (2021b). Mapping soil arching-induced shear and volumetric strains in dense sands. *Transportation Geotechnics*, 28, 100547.
- Lee, C. J., Wu, B. R., Chen, H. T., & Chiang, K. H. (2006). Tunnel stability and arching effects during tunneling in soft clayey soil. *Tunnelling and Underground Space Technology*, 21(2), 119–132.
- Li, R., Zhang, D. L., Song, Y., Li, A., & Luo, J. W. (2023). Pressure arch effect of deeply buried symmetrically distributed triple tunnels. *Symmetry*, 15(3), 673.
- Liang, L. J., Xu, C. J., Chen, Q. Z., & Chen, Q. S. (2020). Experimental and theoretical investigations on evolution of soil-arching effect in 2D trapdoor problem. *International Journal of Geomechanics*, 20(6), 06020007.
- Lin, X. T., Chen, R. P., Wu, H. N., Meng, F. Y., Su, D., & Han, K. (2021). Calculation of earth pressure distribution on the deep circular tunnel considering stress-transfer mechanisms in different zones. *Tunnelling and Underground Space Technology*, 119, 104211.
- Liu, C., Zhang, Z. X., & Regueiro, R. A. (2014). Pile and pile group response to tunnelling using a large diameter slurry shield – Case study in Shanghai. *Computers and Geotechnics*, 59, 21–43.
- Ministry of Water Resources of the People's Republic of China. (2019). *GB/T 50123–2019: Standard for geotechnical testing method*, Beijing. (in Chinese).
- Ministry of Housing and Urban-Rural Development of the People's Republic of China. (2021). *GB/T 51438–2021: Chinese standard for design of shield tunnel engineering*, Beijing. (in Chinese).
- Rui, R., Tol, F. V., Xia, Y. Y., Eekelen, S. V., & Hu, G. (2018). Evolution of soil arching: 2D analytical models. *International Journal of Geomechanics*, 18(6), 04018056.
- Schanz, T., & Vermeer, P. A. (1996). Angles of friction and dilatancy of sand. *Géotechnique*, 46(1), 145–151.
- Song, X., Meng, F. Y., Chen, R. P., Wang, H. L., & Wu, H. N. (2023a). Effect of seepage on soil arching effect in deep shield tunnel. *Underground Space*, 12, 218–233.
- Song, X., Wu, H. N., Meng, F. Y., Chen, R. P., & Cheng, H. Z. (2023b). Soil arching evolution caused by shield tunneling in deep saturated ground. *Transportation Geotechnics*, 40, 100966.
- Terzaghi, K. (1943). *Theoretical soil mechanics*. New York: John Wiley & Sons.
- Tiwari, B., Ye, G. L., Li, M. G., Khalid, U., & Yadav, S. K. (2020). Strength and dilatancy behaviors of deep sands in Shanghai with a focus on grain size and shape effect. *Journal of Rock Mechanics and Geotechnical Engineering*, 12(6), 1214–1225.
- Wong, R. (1986). *Design and performance evaluation of tunnels and shafts*. [Doctoral dissertation, The University of Alberta, Edmonton].
- Wu, C. S., & Zhu, Z. D. (2018). Comparative study on ground loss ratio due to shield tunnel with different diameters. *Chinese Journal of Geotechnical Engineering*, 40(12), 2257–2265 (in Chinese).
- Wu, J., Liao, S. M., & Liu, M. B. (2019). An analytical solution for the arching effect induced by ground loss of tunneling in sand. *Tunnelling and Underground Space Technology*, 83, 175–186.
- Xiong, H., Qiu, Y. Y., Lin, X. T., Chen, X. S., & Huang, D. W. (2023). Multiple arching in cohesion–friction soils: Insights from deformation behavior and failure mechanisms using FEM-SPH approach. *Computers and Geotechnics*, 154, 105146.
- Xiong, H., Qiu, Y. Y., Shi, X. S., Wang, X., & Chen, X. S. (2024). Arching development above active trapdoor: Insight from multi-scale analysis using FEM–SPH. *Acta Geotechnica*, 19(5), 2419–2443.
- Zhang, H. F., Zhang, P., Zhou, W., Dong, S., & Ma, B. S. (2016). A new model to predict soil pressure acting on deep burial jacked pipes. *Tunnelling and Underground Space Technology*, 60, 183–196.